batteries

Article

Centralized SoC Balancing for Batteries with Droop-Controlled DC/DC Converters for Electric Aircraft

Elias Berschneider [1,2,*], Bernhard Wagner [2], Markus Meindl [1] and Bernd Eckardt [1]

[1] Department Power Electronics, Fraunhofer Institute for Integrated Systems and Device Technology IISB, 91058 Erlangen, Germany
[2] Fakultät EFI, Technische Hochschule Nürnberg, 90489 Nürnberg, Germany
* Correspondence: elias.berschneider@iisb.fraunhofer.de

Abstract

In this article, an approach to balance the State of Charge (SoC) of two batteries connected to the DC bus of a fuel cell (FC) electric aircraft by Droop-controlled converters is described. The proposed algorithm is based on shifting the Droop reference voltages and prevents the simultaneous charging and discharging of the batteries. This approach is not only practical but also highly versatile, as it is compatible with all converters as long as the Droop voltage can be changed remotely, and a current measurement is provided to a central controller. No further programming access to the DC/DCs is necessary. There is no need for nonlinear or different-valued Droop resistances for charging and discharging. The balancing approach is validated via simulation in MATLAB/Simulink 2024a.The results show that the proposed approach achieves SoC balancing without degrading the dynamic performance of the grid. The delays added by the slower communication with the central controller have a minimal impact on performance.

Keywords: battery management system; centralized control; DC microgrids; Droop control; electric aircraft; SoC balancing

Academic Editors: King Jet Tseng and Pascal Venet

Received: 31 July 2025
Revised: 6 October 2025
Accepted: 4 November 2025
Published: 6 November 2025

Citation: Berschneider, E.; Wagner, B.; Meindl, M.; Eckardt, B. Centralized SoC Balancing for Batteries with Droop-Controlled DC/DC Converters for Electric Aircraft. *Batteries* **2025**, *11*, 411. https://doi.org/10.3390/batteries11110411

1. Introduction

The move towards more electric aircraft has been ongoing for some time. Many auxiliary functions that were previously powered hydraulically—using pumps mechanically coupled to the turbines—or pneumatically, using bleed air, have been replaced by electric actuators in newer aircraft [1,2]. In contrast, the development of fully electric aircraft, which use no combustion engines, and hybrid-electric aircraft, where part of the propulsive power is provided by electric drives in addition to conventional turbines, is still at an early stage for commercial applications. Significant improvements are still required in terms of the component power density, the energy density of storage systems, and the development of airport infrastructure to make these concepts—particularly fully electric aircraft—viable [3–5]. While all-electric wide-body aircraft remain unrealistic without major technological breakthroughs [6], the development of short-range commuter-class aircraft is considered an achievable goal [7]. In this article, an SoC-balancing method is proposed, developed specifically for a small fully electric aircraft. While batteries are often part of the auxiliary power unit in more-electric aircraft, they generally play a minor role compared to turbine-driven generators, as the architectures shown in [6] demonstrate. However, in hybrid or fully electric aircraft, high-voltage (HV) batteries are indispensable. In the case of fuel-cell electric aircraft, HV batteries are essential, since the dynamics of fuel-cell systems are not fast enough to stabilize the grid during

transients. For aircraft applications, the use of multiple smaller-capacity batteries instead of a single large battery is a standard practice in order to avoid single points of failure. Consequently, the power output and SoC of the batteries must be balanced to prevent unequal degradation of the battery system and to ensure that all batteries maintain a sufficiently high SoC to stabilize the grid in case one storage unit fails. Although different control strategies for DC microgrids exist, which have been reviewed in [8,9], for the primary bus voltage control, Droop control is often employed. Due to the influence of line impedances on DC Droop control, a secondary control layer is generally required to achieve accurate power sharing between parallel converters. This decentralized voltage control scheme offers inherent advantages in the event of communication failure with a central energy management system (EMS). While Droop methods with complex impedances that take the dynamics of different sources like fuel cells and super caps into account have been proposed [10], the standard is still based on either power and voltage or voltage and current with a fixed Droop coefficient [11]. By contrast, a decentralized SoC-balancing and power-sharing scheme is not strictly necessary, as the grid can continue operating without it under failure conditions. Thus, a hierarchical control approach with decentralized voltage control and rough load distribution via Droop control and optimization by an EMS offers both reliable main control during faults and efficiency under normal operating conditions. Especially in onboard grids, where a communication link between sources is already available, a centralized approach entails few disadvantages. Moreover, decentralized SoC balancing requires access to the software of the battery DC/DC converters, which may not be feasible if the converters are sourced externally.

In this article, a novel SoC-balancing algorithm is proposed for a DC grid with Droop-controlled battery storage systems, based on shifting the reference voltages. The algorithm is executed entirely on a central EMS and requires only the adjustment of the Droop voltage and a linear Droop resistance of the DC/DC converters. Therefore, it is compatible with any DC/DC converter used in such grids.

2. Materials and Methods

The powertrain architecture of the specific aircraft, which forms the basis of this study, consists in actuality of two separate powertrains each with a single battery and FC of each wing. This allows to isolate potential failures to only part of the system. But both powertrains can be connected during operation. This can be used to balance the thrust between the wings, for example, if the FC of one side fails, the power of the second can be distributed evenly to the motors on both sides. As the SoC balancing only becomes important if the powertrains are connected, only this configuration will be used. Furthermore, how the power is distributed between the different loads and FCs does not affect the balancing—only the combined values are of importance. Thus, the simplified model in Figure 1 will be used for the analyses.

Here, two battery systems are connected to the central HV-bus by boost converters. These batteries primarily stabilize the bus voltage and provide additional power to the bus during periods of high drive demand, such as take-off. For most of the time, the fuel cell supplies most of the power to the bus. The power set-point and the set-points for the battery DC/DCs are provided by an algorithm on the central energy management system (EMS). This EMS also receives inputs from the flight controller fuel cell management system (FCMS) and battery management system (BMS), which provides data about the batteries, such as the SoC. To balance the SoC between these battery systems, many methods have been suggested in the literature. Use of adaptive Droop control to balance SoCs is common in the literature [12,13]. An overview and review of many of those approaches is provided in [14]. In the paper, a variety of both centralized and decentralized SoC-balancing methods

are shown. However, most of the Droop-based techniques shown rely on varying the Droop resistance, which often involves nonlinear or piecewise linear Droop curves like those presented in [15–23]. Therefore, those approaches are not suitable for operation with DC/DCs, where only a single value for the droop resistance can be set. A method of balancing the SoC by varying the reference voltage has also been shown in [24]. In this approach, both the SoC and the current output power of the battery storage systems affect the reference voltage of the converters linearly. By applying this approach, it is not necessary to use different Droop resistances for charging and discharging. However, if the reference voltages are not all the same, operating points can occur in which one battery charges while another discharges. This is especially relevant when the batteries provide little power to the bus. This can be observed in Figure 2, where a similar balancing scheme is employed.

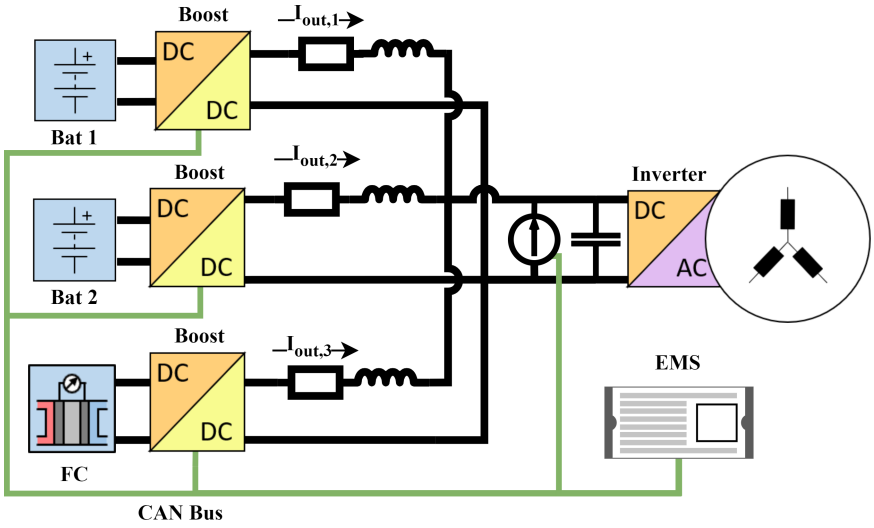

Figure 1. Overview of the studied grid.

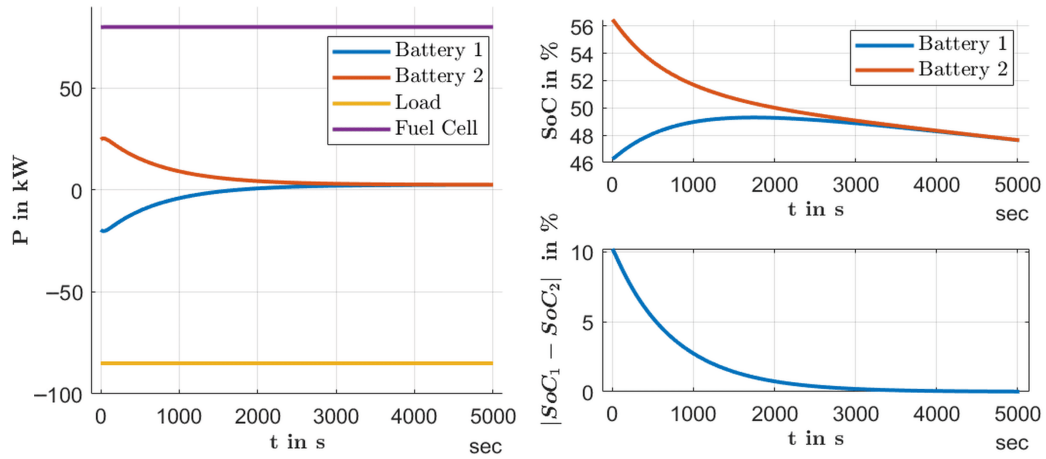

(**a**) (**b**)

Figure 2. (**a**) Power balance of the HV bus and (**b**) SoC of the batteries with linear-cubic function with a saturation reference voltage shift-based SoC-balancing algorithm (positive power is flowing to the bus).

The first battery is charging while the second battery is discharging until the SoCs of the battery systems are mostly equalized. Due to the unnecessary losses this causes, this is especially an issue for mobile applications, where efficiency is of even greater importance. This can be mitigated to an extent by reducing the shift in the reference voltage. However, it is an issue that is inherent to this approach to SoC balancing. In the following paragraphs, the impact of different functions for calculating the reference voltage shift of the DC/DCs is investigated, and an additional logic is presented, which avoids the issue of circulating currents entirely.

3. Basic Balancing Algorithm

At first, a simple algorithm is presented. It calculates the shift in the reference voltage V_{Droop} for both batteries DC/DC converters based on the SoC measurements. The conventional Droop equation is given as:

$$V_{DC,n} = V_{ref,n} - R_D \cdot i_{out,n} \tag{1}$$

where $V_{DC,n}$ is the output of the Droop equation, which is used as the setpoint for the voltage control loop of the n-th DC/DC converter. $V_{ref,n}$ is the reference voltage of the n-th converter, $i_{out,n}$ is the output current measured by the DC/DC, and $R_{D,n}$ is the Droop resistance of the converter. In this case, $R_{D,n}$ and $V_{ref,n}$ are the same for all Droop-controlled DC/DCs. The control scheme of the converters can be seen in Figure 3.

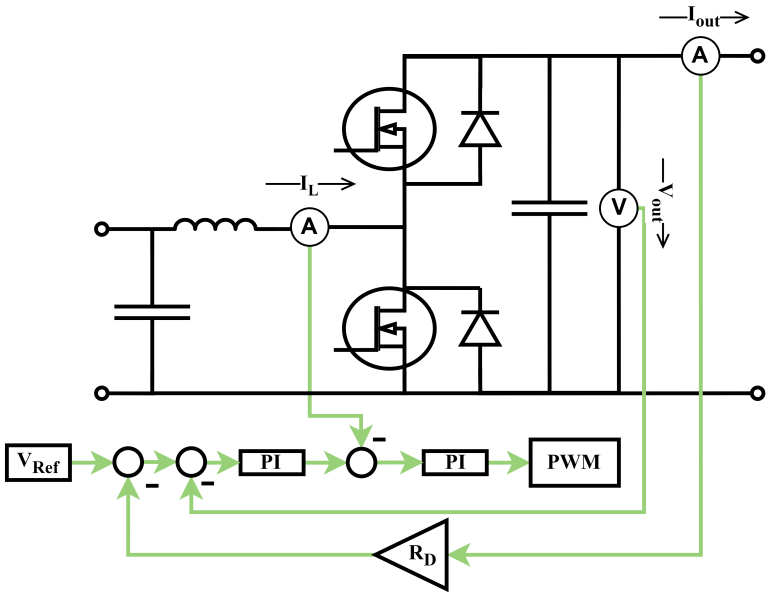

Figure 3. Model of the batteries with the control loop and internal measurements.

The balancing algorithm substitutes $V_{ref,n}$ with $V*_{ref,n}$. This value is computed taking ΔSoC in to account, with ΔSoC calculated to be:

$$SoC_{avg} = \frac{\sum_{i=1}^{n} SoC_n}{n} \tag{2}$$

$$\Delta SoC_n = SoC_n - SoC_{avg} \tag{3}$$

To achieve the desired equalization of the SoCs while maintaining voltage control accuracy, certain constraints must be imposed on the function calculating $V*_{ref,n}$. At first, the average $V*_{ref,n}$ must be V_{ref}. This ensures the voltage set point of the entire grid is not affected by the SoC balancing. For the case with two battery systems that is investigated here, this means $|V*_{ref,n} - V_{ref}|$ must be the same for both batteries.

Secondly, a maximum value for $|V*_{ref,n} - V_{ref}|$ for the maximum of ΔSoC_n must be chosen. This is due to the adverse effect a significant shift in $|V*_{ref,n} - V_{ref}|$ can have on the voltage control accuracy. This can be observed by looking at the added Droop curves, as this represents the resulting Droop curve from the perspective of the HV bus. Examples of this can be seen in Figure 4. In Figure 4a, the reference voltages have been shifted further apart. In this case, the current limitation of the DC/DCs results in the combined Droop curve being zero around V_{ref}, which reduces the accuracy of V_{bus}. In contrast, in Figure 4b, the shift in the reference voltages is smaller, and as such, the combined Droop curve does not plateau in the region around V_{ref}. In the regions where one DC/DC already outputs its maximum current while the other does not, the resulting Droop resistance also increases. In this case, a region around V_{ref}, where the resulting Droop curve is zero, is undesirable. This puts a limit on $|V*_{ref,n} - V_{ref}|$. This value can be calculated as in Equations (4) and (5).

$$SoC_{avg,maxDiff} = \frac{SoC_{min} + \sum_{i=1}^{n-1} SoC_{max}}{n} \tag{4}$$

$$|\Delta SoC_{max}| = |SoC_{min} - SoC_{avg,maxDiff}| \tag{5}$$

For a case with two batteries, an SoC_{min} of 0% and an SoC_{max} of 100%, $|\Delta SoC_{max}|$ equates to 0.5 for the unlikely case that one battery is fully charged while the other is fully discharged. The maximum value for $|V*_{ref,n} - V_{ref}|$ can be calculated as shown in Equation (6), where V_{Droop} represents the width of the voltage region, where the Droop is active. In this case, $V_{ref} = 830$ V, and the voltage band is between 810 V and 850 V.

$$V_{ref,max/min} = V_{ref} \pm \frac{V_{Droop}}{2} \tag{6}$$

In the studied case, this leads to the constraint on $f_{Balancing}(\Delta SoC_n)$ shown in Equation (7).

$$830\text{ V} \pm 20\text{ V} \stackrel{!}{=} f_{Balancing}(\pm 0.5) \tag{7}$$

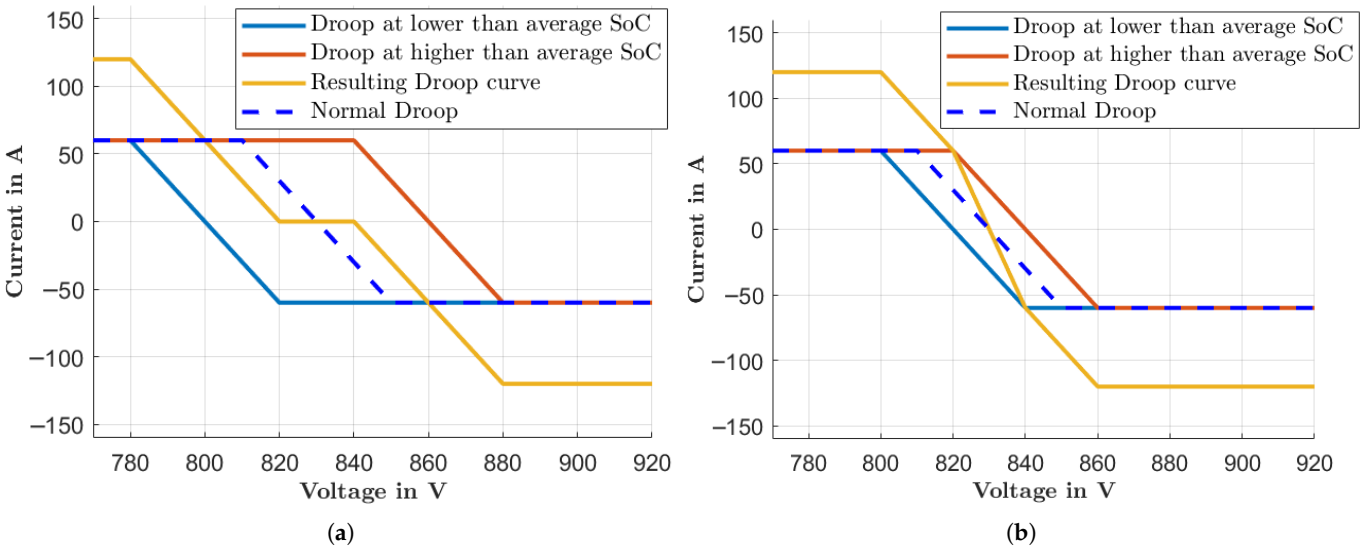

Figure 4. Impact of the shifted Droop curves on the combined Droop curve. (**a**) Large shift in V_{ref}; (**b**) small shift in V_{ref}.

Next, a function type needs to be chosen. For this case, odd-order polynomials or roots are especially suited due to their point symmetry. This allows for the use of the same function for positive and negative values of ΔSoC_{max}. The functions must be

monotonous and can be easily manipulated to fit the previously stated requirements. In Figure 5, different potential candidates for $f_{Balancing}(\Delta SoC_n)$ are shown. These functions are further investigated. The coefficients were set at values which fulfill the requirement set in Equation (7). In the case of the mixed cubic and linear function depicted in purple, the requirements have been changed. In this case, the coefficients were determined so that Equations (10) and (12) are satisfied. From Figure 5, it is clear that the function based on the cube root leads to the fastest convergence of the SoCs, as the difference in the $V*_{ref,n}$ is larger across all ΔSoC_n.

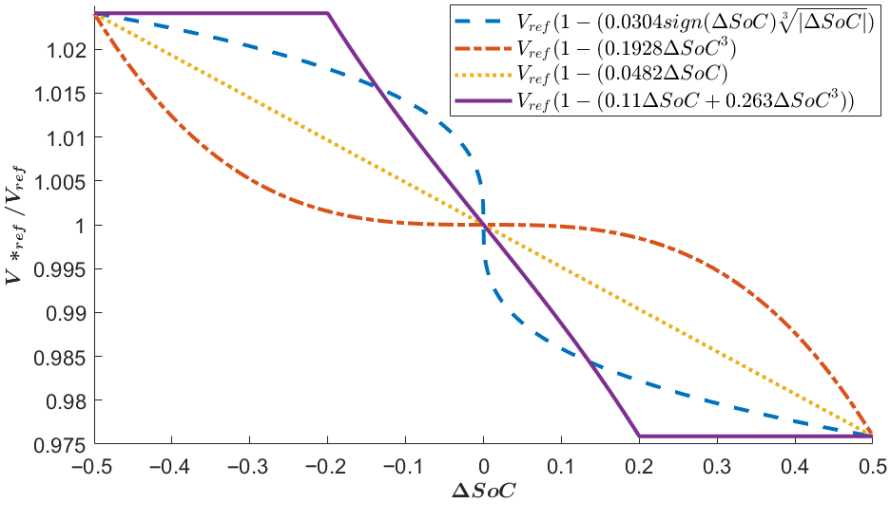

Figure 5. Investigated candidates for the function $V*_{ref,n} = f_{Balancing}(\Delta SoC_n)$.

However, due to this, the derivative of the function is especially large up to infinity in the region around $\Delta SoC_n = 0$. This leads to cases where the power outputs of the batteries vastly differ, even if the SoCs are similar. Depending on the accuracy of the SoC measurement, this causes an unnecessary load on the batteries. Due to the low rate of change of the SoC, this also leads to an overshoot of the SoC balancing and subsequent oscillations. This can be observed in Figure 6a,b. An overshoot in the SoC balancing is an undesirable effect, which rules this function type out.

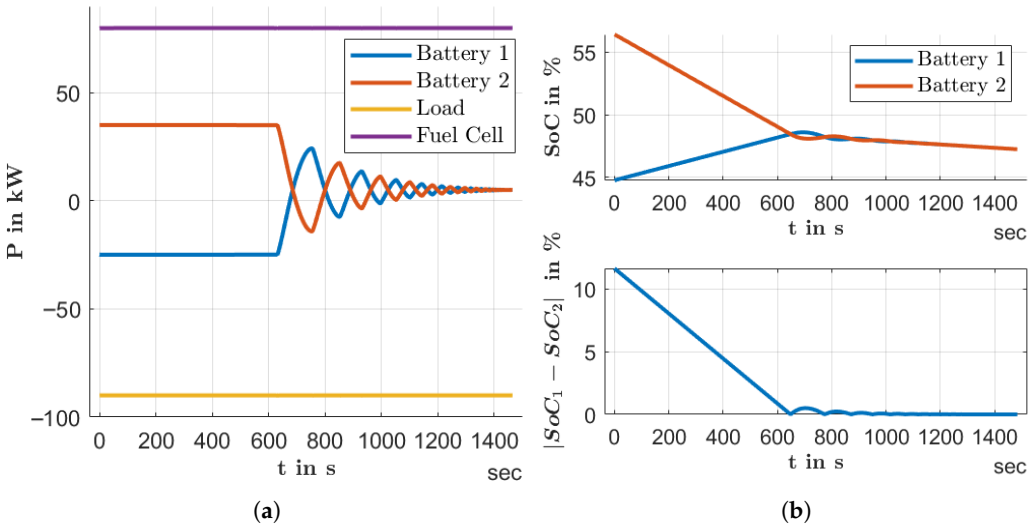

(**a**) (**b**)

Figure 6. Convergence of battery DC/DC output power with SoC balancing based on cube root function. (**a**) Power over time; (**b**) SoC over time.

A linear function leads to a slower equalization of the SoCs than the cube root function, as is depicted in Figure 7a. However, this is sufficient for many applications.

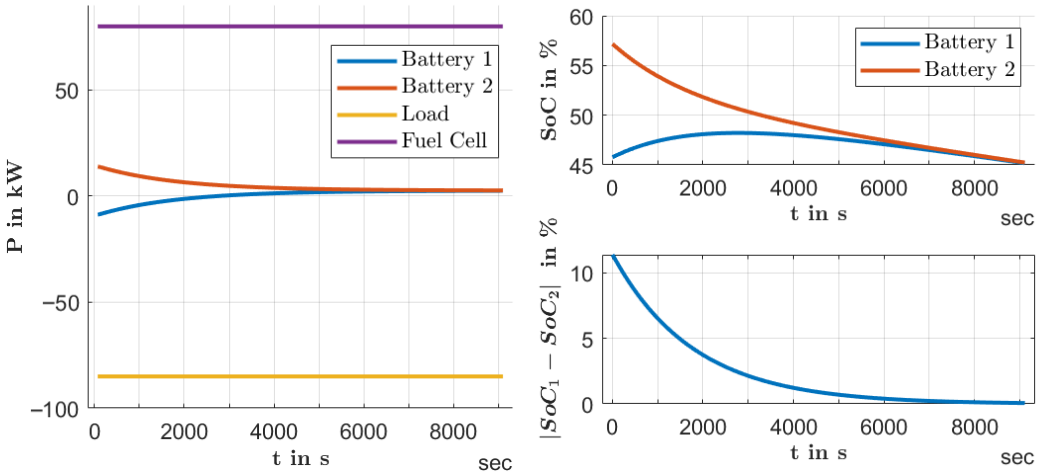

(**a**) (**b**)

Figure 7. Convergence of battery DC/DC output power with SoC balancing based on the linear function. (**a**) Power over time; (**b**) SoC over time.

The cubic without a linear part function achieves the slowest equalization of all functions investigated. As is depicted in Figure 8b, the difference in the SoCs between the two batteries remains virtually the same over the timespan of the simulation. The difference in power output between the two batteries similarly remains almost constant at ca. 200 W throughout the simulation. A balancing based on this function is thus too slow for this application. Additionally, the difference of ca. 200 W in output power of the batteries corresponds, combined with a small Droop resistance, only to a slight shift in the reference voltage. This can pose practical issues, as in practice, the reference voltage of the DC/DCs can only be set to a certain accuracy. In the simulation shown in Figure 8a, the difference in the reference voltages of the DC/DCs is only of the order of tens of mV. This can be determined by evaluating the cubic function shown in Figure 5. At SoC of 55% and 47 %, respectively, this leads to a $\Delta SoC_{1/2}$ of ∓ 0.04. The difference between the reference voltages can then be calculated as in Equation (8).

$$|2(825 - 825 \cdot (1 - (0.1928 \cdot (\mp 0.04)^3)))| = 0.02 \text{ V} \tag{8}$$

This accuracy is not achievable in reality. As such, even if the slow equalization of the battery SoCs achieved with the cube function might be acceptable for specific applications, it is unsuitable due to the practical restrictions on the control accuracy of a DC/DC.

Thus, of the simple linear, cube, and cuberoot functions investigated, only the linear function offers an equalization of the SoCs without serious drawbacks. However, if a faster equalization is required while still keeping the restrictions imposed on the maximum and minimum values of $V*_{ref}$, a saturation can be used. In this case, a fast equalization is advantageous, as the algorithm preventing simultaneous charging and discharging slows the equalization down. For this function, a linear and cubic part are combined in addition to the saturation. This leads to a function in the form of Equation (9).

$$f_{Balancing}(\Delta SoC_n) = V_{ref}(1 - (k_1 \Delta SoC_n{}^3 + k_2 \Delta SoC_n)) \tag{9}$$

$$\frac{V*_{ref,max/min}}{V_{ref}} = (1 - (k_1(\pm \Delta SoC_{lim})^3 + k_2 \Delta \pm SoC_{lim})) \tag{10}$$

$$\left.\frac{df_{Balancing}(0)}{d\Delta SoC_n}\right|_{max} = k_2 \tag{11}$$

$$k_1 \geq 0, k_2 \geq 0 \tag{12}$$

Due to constrictions imposed before, the values of k_1 and k_2 can be chosen freely to achieve the desired behaviour as long as the conditions in Equations (10) and (11) are fulfilled. Hereby, $\pm\Delta SoC_{lim}$ denotes the value of ΔSoC_n, where $f_{Balancing}(\Delta SoC_n) = V*_{ref,max/min}$. Here, $\pm\Delta SoC_{lim}$ is set at ± 0.2, which equates to a difference in the SoC between the batteries of 40%. The maximum value of k_2, where the balancing does not lead to an overshoot, was empirically determined to be around 0.11. This leads to a value of 0.263 for k_1. As can be seen in Figure 4, the cube part has little impact on the function and could be omitted if the restrictions on $\pm\Delta SoC_{lim}$ are dropped. As can be seen in Figure 2, this function leads to a faster convergence of the SoCs than the linear function depicted in Figure 7 while avoiding the oscillations of the cube root function depicted in Figure 6. However, it is also clear from Figure 5 that the faster convergence of the SoCs is mostly due to the increase in the linear part of the function. If the strict conditions put on the function are weakened by allowing a slight deviation for $\pm\Delta SoC_{lim}$, a similar outcome can be achieved without the cubic part of the function. Thus, this function is the most advantageous of those investigated and will be used further on.

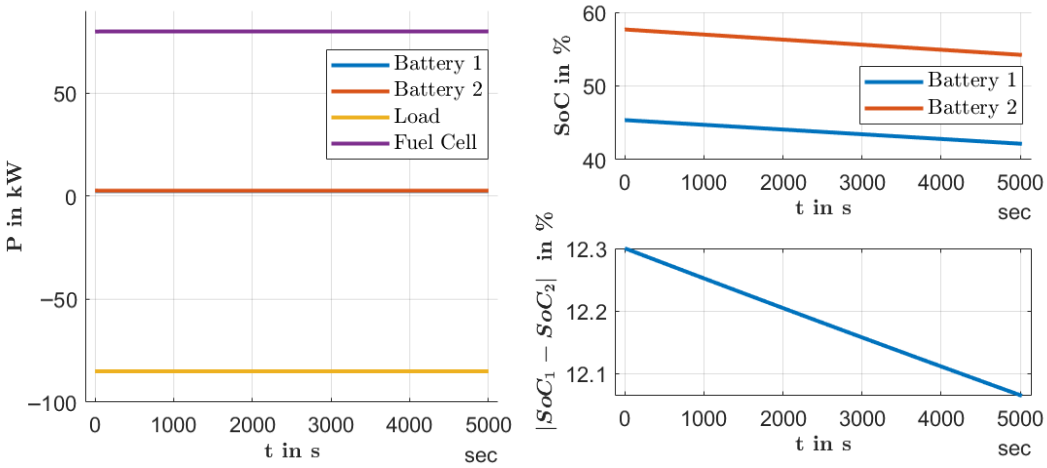

(**a**) (**b**)

Figure 8. Convergence of battery DC/DC output power with SoC balancing based on the cube function. (**a**) Power over time (Note: power of Battery 1 and 2 is almost identical); (**b**) SoC over time.

4. Additional Algorithm Preventing Simultaneous Charging and Discharging

As previously stated, an issue with this method of balancing the SoC of multiple batteries arises due to a shift in the voltage set points. This can lead to some batteries being charged while others are discharging. This can be seen in Figures 4 and 7. The reasons for this can be seen in Figure 9. Here, an operating point is depicted where the batteries' combined output is 20 A. In this graphic, the current in the operating point can be determined from the intersection of the vertical dotted line with the respective Droop curve. In the case of the battery with lower SoC, this is the blue curve and for the battery with higher SoC, it is the red curve. The resulting Droop depicted in the orange curve is then the addition of both curves. Were the Droop curves are not shifted, both battery DC/DCs would ideally output half of the current. As the balancing shifts, the Droop curves symmetrically, while the combined current stays the same. However, due to shifted Droop curves, the battery with the lower SoC would draw current from the bus while the battery with the higher

SoC supplies this current in addition to the current supplied to the bus. Such operating points mainly occur when the power demand of the loads is close to the power provided by sources other than the batteries, or if the SoCs diverge significantly. In the case of the application for aircraft, these operating points occur frequently as the batteries are mainly used for stabilization of the bus with no or only a small power output during cruise of the aircraft.

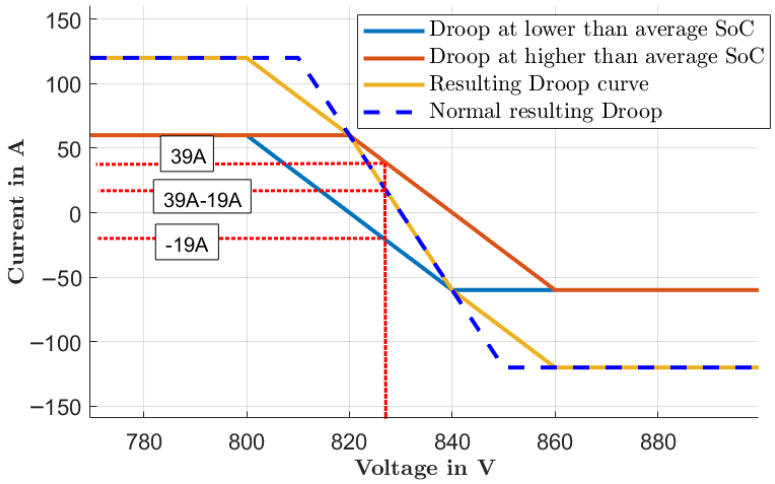

Figure 9. Exemplary operating point with one battery charging and another discharging.

This behavior can be desirable if a fast convergence of the SoCs is required. However, in most cases, this shifting of energy between batteries leads only to unnecessary additional losses and inefficiencies. As such, additional logic is added to the balancing algorithm to prevent such operating modes. Once the SoCs of the batteries deviate less than a given value and one battery charges while the other discharges, the output current of the battery that outputs the smaller current in absolute terms is set to zero. As the bus tie DC/DC converters need to stay in Droop control mode to stabilize the grid in case transients occur, this is achieved by setting the reference voltage of the Droop controller to the bus voltage. However, this also changes the operating point of the entire grid. In the new operating point, the battery whose output was set to zero might no longer be the one with the smaller output current by the logic of the original Droop control. As such, the reference voltage of the other battery needs to be adjusted as well to ensure the sum of the power supplied to the bus by the batteries stays constant. If this is not done, the operating point might start to oscillate.

The logic consists of two parts—one for determining, whether one battery current should be set to zero, and one to perform this task. The part to detect, if the algorithm should be activated, is depicted in Figure 10.

It checks two conditions. One is comparing the ΔSoC to a set threshold. Only if the deviation of the SoCs is smaller than this value will the simultaneous charging and discharging of the batteries be prevented. This condition is optional and could, in applications where simultaneous charging and discharging is never desired, be removed. As the second condition, it is monitored whether the bus voltage is smaller or greater than $V*_{ref,n}$. At this voltage, the battery outputs zero current. This holds true irrespective of the line impedances. If the signs of the differences between $V*_{ref,n}$ and the bus voltage V_{Bus} are not equal, the battery currents will also have different signs. With an even number of batteries, this can be done by comparing the product of the differences to zero. However, for practical reasons, the product of the subtractions is not compared to zero but a small positive value like 0.1, as shown in Figure 10. If the voltage fluctuates, and accounting for measurement accuracy, this logic might otherwise activate and deactivate. If both requirements are met,

the second part of the logic activates. This part of the logic is depicted in Figure 11. It finds the converter with the smaller output current and feeds the solution or its inverse in NAND gates with the second input being the solution of the detection logic. The output currents $I_{out,n}$ are fed into PI controllers both as set points and as control deviation. The set points are multiplied by the outputs of the NAND gates. This means the input of a PI controller is zero if the NAND gate is true. This is the case if the detection logic does not detect simultaneous charging and discharging. Or—if it is detected—if $I_{out,n}$ of the respective converter is bigger. If the PI input is zero, its output is zero as well, because whenever a NAND output changes, the integrators of the controllers are reset. The NAND gates control switches as well. If simultaneous charging and discharging is not detected, $V*_{ref,n}$ is directly passed through to $V**_{ref,n}$. If is detected that $|I_{out,n}|$ of a given converter is smaller, $V**_{ref,n}$ equals the output of the PI controller, which takes I_{out} of the same converter as input, plus $V*_{ref,n}$. Otherwise, $V**_{ref,n}$ is $V*_{ref,n}$ minus the output of the PI controller connected to I_{out} of the other converter. This way, the Droop curves of both converters are shifted by the same absolute voltage value but with different signs. Thus, the combined output current remains constant. This situation is depicted in Figure 7. There, simultaneous charging and discharging is detected and $I_{out,2}$ is smaller. In this example, $V**_{ref,1}$ is equal to the output of PI_1 plus $V*_{ref,1}$, whilst $V**_{ref,2}$ is the difference in $V*_{ref,2}$ minus the output of PI_1.

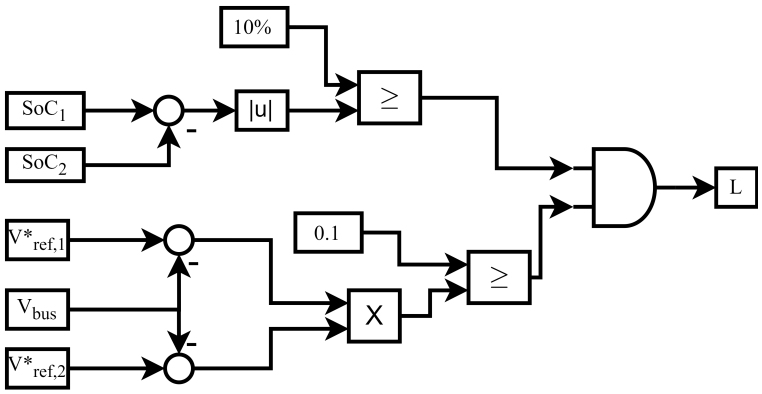

Figure 10. Detection logic.

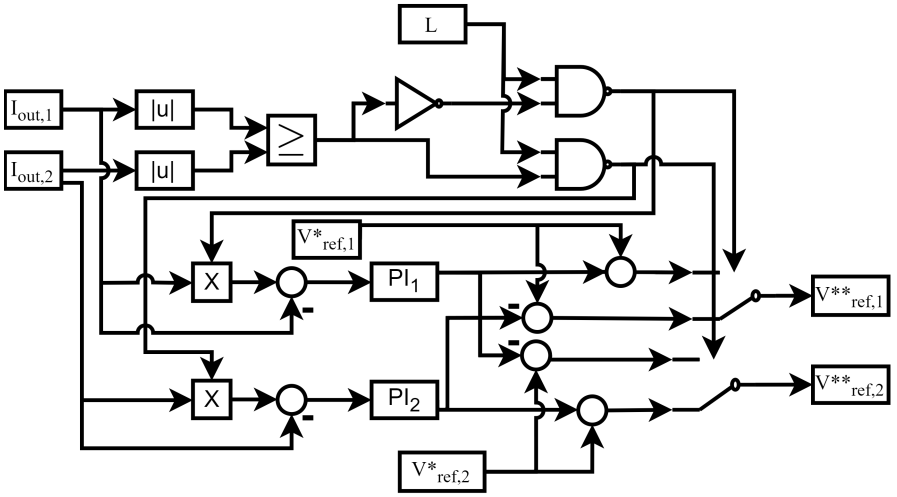

Figure 11. Control logic.

5. Parameters of the Studied Grid

The configuration of the grid with which this approach to SoC balancing was tested is shown in Figure 1. This shows a fuel cell electric powertrain with a single fuel cell and two batteries, all of which are connected to the HV bus by boost converters. Connected to the HV bus is a single constant power load (CPL) representing a motor. In the simulation, the fuel cell constantly produces 80 kW while the motor power, represented by a CPL, is changed throughout the simulation. The power output of the batteries is controlled by Droop controllers throughout the simulation. The values of currents, voltages, and SoCs are sampled by the balancing algorithm every 100 ms, representing the delay introduced by communication via CAN. To calculate the shift in the reference voltages, the linear-cubic function with saturation previously shown is used with the values 0.263 for k1 and 0.11 for k2, as depicted in Figure 5.

6. Simulation Results

As a first scenario, the grid is simulated at a steady operating point with a constant load of 85 kW to show the effect of the battery balancing. This leads to a combined power demand from the batteries of 5 kW. This means that if only basic balancing was used, the batteries would charge and discharge simultaneously until the deviation of the SoCs becomes relatively small. For the simulation, the batteries start with an SoC of approx. 47% and 55%, respectively. The other parameters of the model relevant for the simulations are listed in Table 1.

Table 1. Parameters of the grid model.

Parameter	Value
SoC Battery 1	47%
SoC Battery 2	55%
V_{ref}	830 V
R_D	150 mΩ
$\frac{V_{ref,max}}{V_{ref}}$	1.024
P_{FC}	80 kW

As shown in Figure 2, due to the balancing without the additional logic, the operating points of the batteries differ drastically. While battery 2, which has the higher charge at the start of the simulation, is discharging at a power of approx. 23 kW, battery 1 is charging at 17 kW. Such an operating point is not desirable in most circumstances due to the increased losses it causes. This can somewhat be mitigated by reducing $V_{ref,max}$, when setting k1 and k2. However, the principal issue is inherent to this balancing approach. The operating point of the batteries quickly converges as the difference in SoC reduces. After ca. 2100 s, both batteries are discharging as the ΔSoC has fallen to 0.5%, which, for most applications, especially once inaccuracies in the SoC measurements are accounted for, is sufficiently small. The simulation shown in Figure 12 starts at the same operating point as in Figure 2; however, the logic preventing the simultaneous charging and discharging is now active. Due to the operating point, the current of battery 1 is controlled to zero. The 0.5% ΔSoC is reached after ca. 7100 s, as can be seen in Figure 12b. As such, the speed of SoC equalization is about 3.4 times slower for this specific operating point than without preventing charging and discharging at the same time. From Figure 12a, it can also be determined that the logic correctly deactivates once the power output to the bus of both batteries has the same direction when evaluating the Droop equations given by the battery balancing.

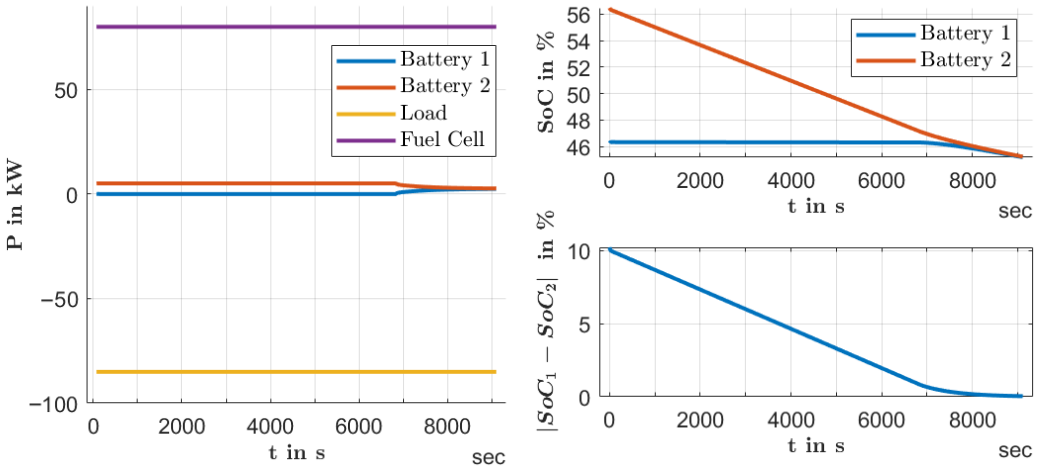

Figure 12. Convergence of battery DC/DC output power with active logic preventing simultaneous charging and discharging. (**a**) Power over time; (**b**) SoC over time.

In addition to the behavior with a constant power demand for the batteries, in a second simulation, the dynamic behavior of this circuit was examined as well. For this, a load change was introduced into the simulation, with a step in the load from 85 kW to 70 kW. This can be seen in Figure 13. Consequently, after the step, the battery current of battery 1 is no longer controlled to zero; instead, the current of battery 2 is. This happens with little delay to the load change. Consequently, the proposed logic is also capable of changing which battery output is controlled to zero. After this, the load is changed back to 85 kW, and then to 100 kW. During this, the current of battery 1 is continually controlled to zero by the logic. As can be seen in Figure 13, this causes only a slight disturbance to the output power of the batteries. This shows that the logic presented is capable of handling transients on the bus.

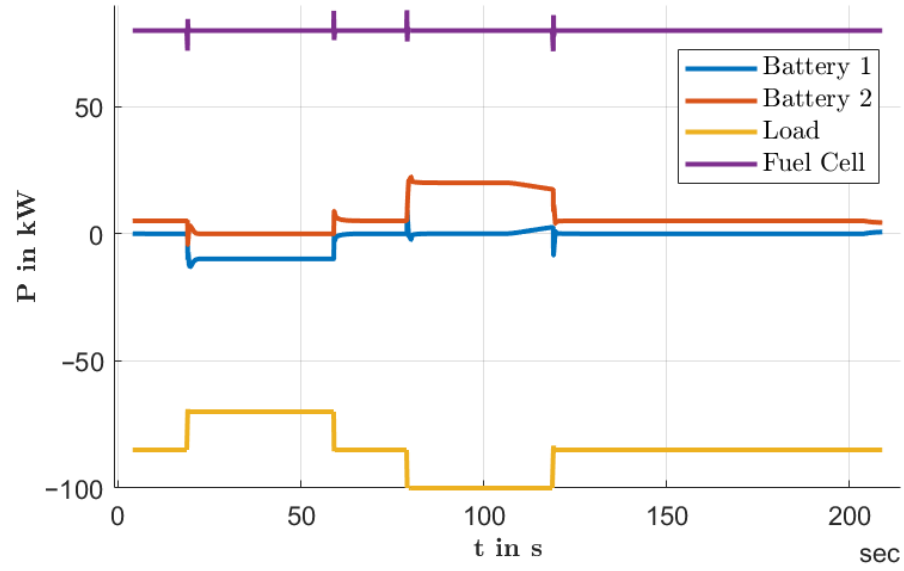

Figure 13. Behavior of the bus during loadchanges.

Analysis of Impact on Energy Efficiency and Performance

As the SoC balancing only affects the currents in the paths between the bus and the two batteries, and since the bus is assumed to be lossless in the model, the combined losses are proportional to the squared sum of the currents, as shown in Equation (13). Similarly, it

follows that the sum of the battery currents must equal the current I_{req} required to satisfy the grid power balance, as in Equation (15). I_{req} can be assumed to be a constant, independent from the SoC balancing, which is derived from the power balance equation under the assumption of a constant bus voltage V_{bus}. This is shown in Equation (14), with P_{Grid} as the load power of the entire grid including losses and P_{FC} as the fuel cell power output. From this, an expression for the optimal relation between the battery currents can be derived, as in Equations (16) and (17). It is evident that the losses are minimized when the battery currents are equal.

$$P_{loss} \propto I_{Bat,1}^2 + I_{Bat,2}^2 \tag{13}$$

$$I_{req} = \frac{P_{Grid} - P_{FC}}{V_{bus}} \tag{14}$$

$$I_{Bat,1} + I_{Bat,2} = I_{req} \tag{15}$$

$$I_{Bat,1}^2 + I_{Bat,2}^2 = (I_{Bat,1} + I_{Bat,2})^2 - 2I_{Bat,1}I_{Bat,2} = I_{req}^2 - 2I_{Bat,1}I_{Bat,2} \tag{16}$$

$$\min_{I_{Bat,1}+I_{Bat,2}=I_{req}} (I_{Bat,1}^2 + I_{Bat,2}^2) = \frac{I_{req}^2}{2} \tag{17}$$

For two batteries of equal capacity, this means that operating without SoC balancing is the most efficient approach. Any SoC balancing will therefore negatively impact the overall energy efficiency. However, it can also be shown that losses are always lower when both battery currents have the same sign, since the term $-2I_{Bat,1}I_{Bat,2}$ remains negative. In this case, the squared sum lies within the interval $[\frac{I_{req}^2}{2}, I_{req}^2]$, whereas it will always exceed I_{req}^2 if the signs differ. This analysis only describes the instantaneous power and not the energy losses, which are proportional to the time integral of the squared sum. To evaluate the efficiency differences between balancing strategies, four scenarios are simulated for each approach: one with simultaneous charging and discharging permitted, and one where it is prevented by an additional algorithm. In each scenario, the power provided to the bus is varied. This is necessary because, with the standard approach, the time span in which the current signs differ decreases as the batteries supply more power to the grid. Conversely, with the additional logic, the ability to balance the SoCs decreases as the power provided by the batteries becomes smaller. This limitation arises because the maximum derivative of ΔSoC is bounded by I_{req}. Such a weakness is inherent in all balancing methods that disallow simultaneous charging and discharging—true of all approaches based on Droop resistance adjustment instead of reference voltage shifting. To overcome this limitation, the load balancing algorithm must intervene. In the studied case, this means adjusting the fuel cell (FC) output power. As shown in Figure 10, the proposed logic also allows deactivation of the algorithm once ΔSoC exceeds a defined threshold. This ensures that ΔSoC remains within acceptable limits, even when the battery power output is small. To demonstrate the differences between them, both approaches are simulated over a fixed time of 6500 s with identical initial SoC values (see Table 1) at the operating points listed in Table 2.

Table 2. Parameters of the tested operating points.

Operating Point Nr.	FC Power	Load Power	I_{req}
1	10 kW	50 kW	48.4 A
2	30 kW	50 kW	24.9 A
3	40 kW	50 kW	12.1 A
4	50 kW	50 kW	00.1 A

The batteries have to supply the power not provided by the fuel cell in addition to the power needed to compensate for the losses of the system. This enables a comparison of both the SoC-balancing speed and the energy efficiency. Evaluating the squared sum integrals over a fixed time rather than only the time to reach a certain ΔSoC threshold also accounts for the fact that a faster balancing method allows operation at the most energy-efficient point for a longer period. As a baseline, a configuration without SoC balancing—where both battery currents are equal—is used. As derived in Equation (17), this represents the most energy-efficient mode of operation. In Figure 14, the square sum integral of the optimum current distribution divided by the square sum integral of either of the two balancing approaches is depicted. This fraction is equal to the relationship of the energy losses. At a value of one, no additional losses are generated compared to the optimum case, while a value of zero means all losses generated are not necessary to fulfill the grid's power demand. It can be seen that preventing simultaneous charging and discharging is more energy-efficient in almost all operating points investigated. Only at high output power does the difference between the two approaches become negligible.

At low power, this efficiency advantage becomes more pronounced. At a combined power demand of about 10 kW, without the additional logic, the optimal losses amount to only about 36% of the observed value. In comparison, with the additional logic, the losses in the optimal case account for around 62% of the observed value. This gap increases further as the power demand decreases. At zero power demand from the grid, the theoretical value of the SoC balancing with the additional logic becomes one as both currents are zero. However, as shown in Figure 15, the efficiency gain comes at the cost of slower SoC balancing. This difference in balancing speed becomes increasingly relevant as the required battery power decreases. At zero battery power demand, no SoC balancing is possible at all if circulating currents are prevented. In Figure 15, this is evident since no convergence time could be determined for the additional logic within the set timeframe at the operating point close to zero power.

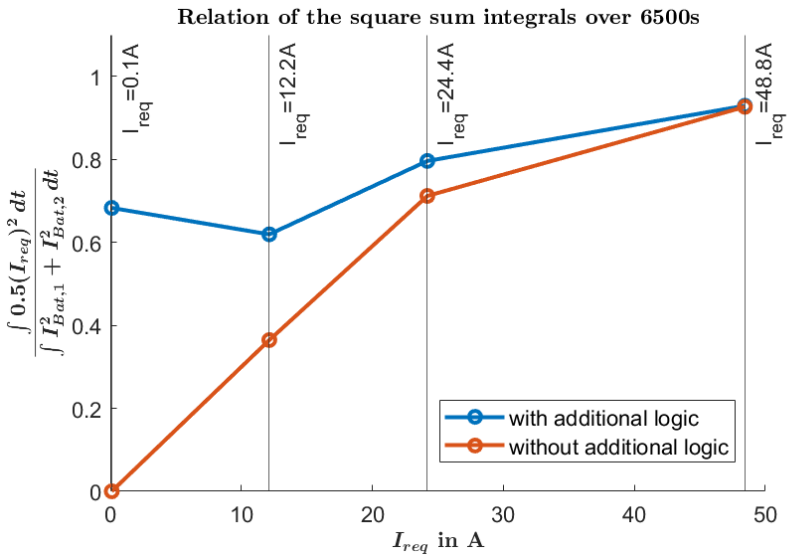

Figure 14. Relation of the squared sum integral of the most efficient current distribution to the squared sum integral of the current distribution with SoC balancing.

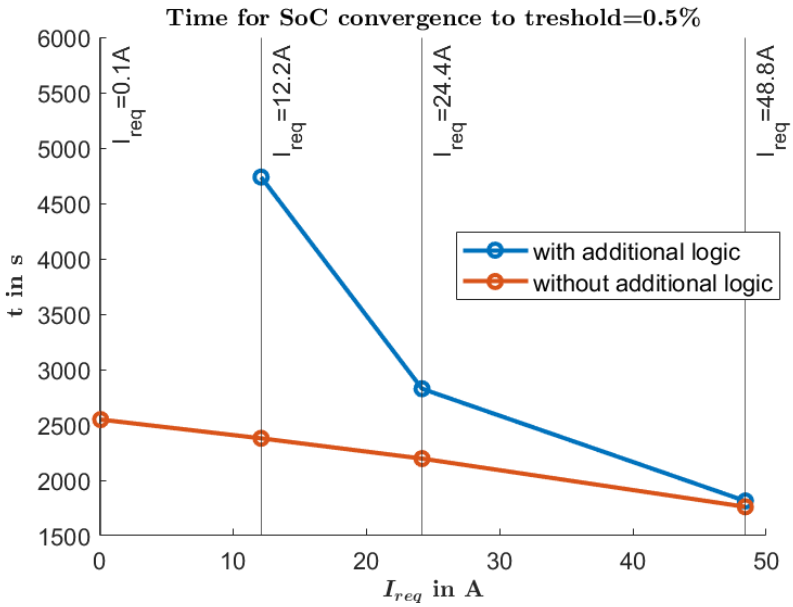

Figure 15. Comparison of the required time to reach an SoC threshold of 0.5% between the standard balancing and the proposed approach

It is, therefore, application-specific to find a compromise between efficiency and balancing speed. For the studied case of a fuel-cell electric aircraft, the slower SoC balancing at low power is an acceptable drawback. The asymmetry of line resistances, which is a major cause of SoC divergence, has a greater effect at high output currents. In the aircraft grid, however, the lines are well characterized, and asymmetries can largely be compensated by the controllers. Large differences in SoC are therefore unlikely to occur. In the conditions where SoC balancing is most critical, the additional logic still performs adequately while offering an overall increase in efficiency.

7. Conclusions

The novel approach to battery SoC balancing consistently equalizes the SoC of two batteries by adjusting the reference voltages of the Droop controller. Since it is fully implemented on a separate EMS, the DC/DC converters do not need to accept nonlinear Droop curves. At the same time, an additional logic was introduced to prevent the issue of undesired simultaneous charging and discharging of different batteries that this method could cause. This is achieved by controlling the reference voltages of the DC/DCs for the batteries. The reference voltage of one DC/DC is set to match the bus voltage to bring its current to zero, while the reference voltage of the other battery's DC/DC is varied by the same absolute value but with the opposite sign. As a result, the total power supplied to the bus remains unchanged. With this, the efficiency of the SoC balancing can overall be increased compared to a standard reference voltage shift SoC balancing but the effectiveness at low power is significantly reduced. Whilst the approach could not be verified with hardware, simulations showed that the detection logic reliably identifies potential circulating currents between the batteries in any operating condition. It was also demonstrated that the proposed algorithm does not negatively affect the grid's transient response, even when considering communication between converters and the EMS. However, it is also clear that the presented SoC-balancing algorithm by its centralized nature is negatively affected by slow communication between the central EMS and the DC/DC converters. A slow or irregular communication affects the presented SoC-balancing approach more negatively than standard methods as the EMS actively controls the output currents. This approach is thus unsuited for grid structures, where the DC/DC control setpoints are not regularly

updated. Additionally, while the SoC balancing is able to reliably reduce differences in charge between the batteries, the actual effectiveness depends on accurate measurements of the battery SoCs like all Droop-based balancing methods. Whilst changes in SoC can be accurately measured by charge counting, the initial battery SoCs often have significant uncertainty. This can lead to unnecessary balancing actions and thus reduce the overall efficiency compared to the presented results. The slow SoC balancing at small differences in battery charges mitigates this issue but does not eliminate it fully. Future work will focus on expanding the balancing algorithm to include more than two batteries for use in larger systems. Additionally, in aircraft applications, the redundant DC/DCs for the batteries will be integrated. Furthermore, the impact of advanced control schemes where fuel cells take a more active role in the grid voltage control by the use of adaptive Droop controllers will be studied. A further verification of the proposed SoC balancing on the demonstrator hardware and realistic load profiles for the application in electric aircraft will be undertaken.

Author Contributions: Conceptualization, E.B.; methodology, E.B.; software, E.B.; validation, E.B., B.W.; formal analysis, E.B.; investigation, E.B.; resources, B.E.; data curation, E.B.; writing—original draft preparation, E.B.; writing—review and editing, E.B., B.W., M.M.; visualization, E.B.; supervision, B.E., B.W.; project administration, B.E.; funding acquisition, B.E. All authors have read and agreed to the published version of the manuscript.

Funding: This study is part of the HYPOTRADE project (https://hypotrade.eu/). The HYPOTRADE project has received funding from the Clean Aviation Joint Undertaking (JU) under Grant Agreement n° 101101998. The JU receives support from the European Union´s Horizon Europe research and innovation program and the Clean Aviation JU members other than the Union. This study only reflects the authors' views; the JU is not responsible for any use that may be made of the information it contains.

Data Availability Statement: The original contributions presented in this study are included in the article. Further inquiries can be directed to the corresponding author.

Conflicts of Interest: The authors declare no conflicts of interest.

Abbreviations

The following abbreviations are used in this manuscript:

BMS	Battery management system
CPL	Constant power load
EMS	Energy management system
FC	Fuel cell
HV	High voltage
SoC	State of charge

References

1. Rosero, J.; Ortega, J.; Aldabas, E.; Romeral, L. Moving towards a more electric aircraft. *IEEE Aerosp. Electron. Syst. Mag.* **2007**, *22*, 3–9. [CrossRef]
2. Buticchi, G.; Wheeler, P.; Boroyevich, D. The More-Electric Aircraft and Beyond. *Proc. IEEE* **2023**, *111*, 356–370. .. [CrossRef]
3. Marciello, V.; Di Stasio, M.; Ruocco, M.; Trifari, V.; Nicolosi, F.; Meindl, M.; Lemoine, B.; Caliandro, P. Design Exploration for Sustainable Regional Hybrid-Electric Aircraft: A Study Based on Technology Forecasts. *Aerospace* **2023**, *10*, 165. [CrossRef]
4. Meindl, M.; de Ruiter, C.; Marciello, V.; Stasio, M.D.; Hilpert, F.; Ruocco, M.; Nicolosi, F.; Thonemann, N.; Saavedra-Rubio, K.; Locqueville, L.; et al. Decarbonised Future Regional Airport Infrastructure. *Aerospace* **2023**, *10*, 283. [CrossRef]
5. Meindl, M.; März, M.; Weber, K.J. Ground-based power supply system to operate hybrid-electric aircraft for future regional airports. In Proceedings of the 2023 IEEE International Conference on Electrical Systems for Aircraft, Railway, Ship Propulsion and Road Vehicles & International Transportation Electrification Conference (ESARS-ITEC), Venice, Italy, 29–31 March 2023; pp. 1–6. [CrossRef]

6. Barzkar, A.; Ghassemi, M. Electric Power Systems in More and All Electric Aircraft: A Review. *IEEE Access* **2020**, *8*, 169314–169332. [CrossRef]
7. Schefer, H.; Fauth, L.; Kopp, T.H.; Mallwitz, R.; Friebe, J.; Kurrat, M. Discussion on Electric Power Supply Systems for All Electric Aircraft. *IEEE Access* **2020**, *8*, 84188–84216. [CrossRef]
8. Al-Ismail, F.S. A Critical Review on DC Microgrids Voltage Control and Power Management. *IEEE Access* **2024**, *12*, 30345–30361. [CrossRef]
9. Modu, B.; Abdullah, M.P.; Sanusi, M.A.; Hamza, M.F. DC-based microgrid: Topologies, control schemes, and implementations. *Alex. Eng. J.* **2023**, *70*, 61–92. [CrossRef]
10. Chen, J.; Song, Q. A Decentralized Dynamic Load Power Allocation Strategy for Fuel Cell/Supercapacitor-Based APU of Large More Electric Vehicles. *IEEE Trans. Ind. Electron.* **2019**, *66*, 865–875. [CrossRef]
11. Qi, L.L.; Gao, M.; Faddel, S. Comparative Study of Four Droop Control Strategies in Buck Converter Based DC Microgrid. *IEEE Trans. Ind. Appl.* **2024**, *60*, 5331–5343. [CrossRef]
12. Li, B.; Yu, C.; Lu, X.; Wang, F. A novel adaptive droop control strategy for SoC balance in PV-based DC microgrids. *ISA Trans.* **2023**, *141*, 351–364. [CrossRef] [PubMed]
13. Luo, Q.; Wang, J.; Huang, X.; Li, S. A Fast State-of-Charge (SOC) Balancing and Current Sharing Control Strategy for Distributed Energy Storage Units in a DC Microgrid. *Energies* **2024**, *17*, 3885. [CrossRef]
14. Fagundes, T.A.; Fuzato, G.H.F.; Silva, L.J.R.; Alonso, A.M.d.S.; Vasquez, J.C.; Guerrero, J.M.; Machado, R.Q. Battery Energy Storage Systems in Microgrids: A Review of SoC Balancing and Perspectives. *IEEE Open J. Ind. Electron. Soc.* **2024**, *5*, 961–992. [CrossRef]
15. Hoang, K.D.; Lee, H.H. Accurate Power Sharing With Balanced Battery State of Charge in Distributed DC Microgrid. *IEEE Trans. Ind. Electron.* **2019**, *66*, 1883–1893. [CrossRef]
16. Zheng, Y.; Tian, G.; Zhang, J. SOC Balancing Control Strategy Based on Piecewise Adaptive Droop Coefficient Algorithm for Multi-energy Storage Units in DC Microgrid. In Proceedings of the 2021 IEEE 4th International Conference on Electronics Technology (ICET), Chengdu, China, 7–10 May 2021; pp. 432–436. [CrossRef]
17. Zhao, R.; Yang, Y.; Zhang, C.; Wei, Z.; Deng, M. Multi-Energy Storage Control Based on SOC for DC-Microgrid. In Proceedings of the 2019 IEEE 4th Advanced Information Technology, Electronic and Automation Control Conference (IAEAC), Chengdu China, 20–22 December 2019; Volume 1, pp. 222–226. [CrossRef]
18. Wu, C.; Wu, C.; Zou, J.; Yan, L. SOC Balance Control Strategy for Distributed Energy Storage System in DC Microgrid. *J. Phys. Conf. Ser.* **2023**, *2655*, 012014. [CrossRef]
19. Mi, Y.; Ma, Y.; Yu, S.; Cai, P.; Ji, L.; Fu, Y.; Yue, D.; Jin, C.; Wang, P. An optimised state-of-charge balance control strategy for distributed energy storage units in islanded DC microgrid. *IET Gener. Transm. Distrib.* **2021**, *15*, 1021–1030. [CrossRef]
20. Ghanbari, N.; Mobarrez, M.; Bhattacharya, S. A Review and Modeling of Different Droop Control Based Methods for Battery State of the Charge Balancing in DC Microgrids. In Proceedings of the IECON 2018—44th Annual Conference of the IEEE Industrial Electronics Society, Washington, DC, USA, 21–23 October 2018; pp. 1625–1632. [CrossRef]
21. Oliveira, T.R.; Gonçalves Silva, W.W.A.; Donoso-Garcia, P.F. Distributed Secondary Level Control for Energy Storage Management in DC Microgrids. *IEEE Trans. Smart Grid* **2017**, *8*, 2597–2607. [CrossRef]
22. Mi, Y.; Guo, J.; Fu, Y.; Wang, C.; Wang, P. Accurate Power Allocation of Multienergy Storage Island DC Microgrid Based on Virtual Power Rating. *IEEE Trans. Power Electron.* **2023**, *38*, 261–270. [CrossRef]
23. Tian, G.; Zheng, Y.; Liu, G.; Zhang, J. SOC Balancing and Coordinated Control Based on Adaptive Droop Coefficient Algorithm for Energy Storage Units in DC Microgrid. *Energies* **2022**, *15*, 2943. [CrossRef]
24. Kewei, C.; Qinfen, L.; Zhanpeng, X. Control Strategy Research on Charge Balancing of Hybrid Energy Storage Units with Islanded Operation Mode of DC Microgrid. In Proceedings of the 2023 IEEE 6th Student Conference on Electric Machines and Systems (SCEMS), Huzhou, China, 7–9 December 2023; pp. 1–7. [CrossRef]